ELSEVIER

International Journal of Solids and Structures 41 (2004) 3707–3733

INTERNATIONAL JOURNAL OF SOLIDS and STRUCTURES

www.elsevier.com/locate/ijsolstr

Quasi-static axial crush response of a thin-wall, stainless steel box component

B.P. DiPaolo [a,*], P.J.M. Monteiro [b], R. Gronsky [c]

[a] US Army Engineer Research and Development Center, 3909 Halls Ferry Road Bldg 5008, Vicksburg, MS 39180-6199, USA
[b] Department of Civil and Environmental Engineering, University of California, Berkeley, CA 94720, USA
[c] Department of Materials Science and Engineering, University of California, Berkeley, CA 94720, USA

Received 14 February 2004; received in revised form 14 February 2004
Available online 20 March 2004

Abstract

An experimental investigation was performed on the quasi-static, symmetric axial crush response mode of commercially-produced, welded AISI 304 stainless steel square box components. The first objective was to demonstrate that a specific configuration response consisting of a fold formation process and the corresponding load–displacement curve could be obtained using experimental control methods. Test specimens from a single length of tubing were examined in a progressive axial crush study, and the controls included removable grooved caps for end constraints, and shallow machined groove patterns on specimen sidewalls for collapse initiators. Consistent fold appearance and load–displacement curve shapes indicated that ten of the eleven test specimens exhibited the same symmetric, axial crush configuration response. During the first cycle of the secondary folding phase, observed differences on an average value basis were less than or equal to 3% for maximum loads, 6% for minimum loads, and 3% for energy absorption. The second objective of this investigation was to isolate the effect of alloy composition and microstructure on the axial crush configuration response. A higher concentration of carbon and smaller grain size resulted in an 18% increase in energy absorption in a secondary folding phase cycle. Overall, the results show that response can be restricted to a specific axial crush configuration response and therefore, a controlled and repeatable energy absorption process can be obtained and modifications to alloy composition and microstructure can be used to enhance energy absorption performance of the box component.

Keywords: Axial crush; Progressive collapse; Thin-wall box components; Stainless steel; Energy absorption; Collapse initiators

1. Introduction

Metallic alloy devices with the ability to irreversibly absorb energy under impact conditions have many important engineering safety applications including crashworthiness and blast resistance. These energy absorption (EA) devices have been investigated with respect to performance quantities, geometry-material

* Corresponding author. Tel.: +1-601-634-4021; fax: +1-601-634-2309.
E-mail address: beverly.p.dipaolo@erdc.usace.army.mil (B.P. DiPaolo).

0020-7683/$ - see front matter © 2004 Elsevier Ltd. All rights reserved.
doi:10.1016/j.ijsolstr.2004.02.031

interdependence, and triggering to initiate and sustain preferred modes of behavior (Coppa, 1968). Designs have been based on structural element responses, modified material processes, and friction (Ezra and Fay, 1972; Johnson and Reid, 1978). Within the structural element category, three major axial EA device responses have been extensively investigated for thin-walled, ductile metallic alloy components subjected to axial compressive loading. These responses depend on energy absorption mechanisms such as plastic deformation, friction, and fracture and are categorized as axial crush (buckling), inversion, and splitting (Reid and Reddy, 1986a). Of the three device responses, the response that is the focus of the current investigation and that relies on the plastic deformation of a progressive fold formation process for the absorption of energy is the one known as axial crush.

Past research has established that axial crush response (see Fig. 1a for an example) is one of several axial collapse responses for thin-walled, ductile metallic alloy tubes with closed cross-sections of simple geometric shapes and subjected to compression loading parallel to the longitudinal axes. Other types of axial collapse response involving plastic deformation include: structural column instability or buckling transitioning to plastic hinge formation; bending collapse even after a number of folds have formed (Mahmood and Paluszny, 1982); elastic local buckling of flat-sided components (Meng et al., 1983) that results in irregular crumpling into panel sections (Mahmood and Paluszny, 1982); and arbitrary localized crumpling (see Coppa, 1968 for example).

Axial collapse responses have been investigated with respect to geometry, material, axial impact velocity and temperature. Studies have been performed on: right-circular cylindrical tubes of alloys of aluminum, brass, copper and stainless steel (Horton et al., 1966; Ren et al., 1983); mild steel and aluminum alloy right-circular cylindrical and square tubes (Macaulay and Redwood, 1964; Redwood, 1964); and low and high strength steel components of right-circular cylindrical and square geometries (VanKuren and Scott, 1978). Additionally, studies have been conducted on aluminum alloy and low carbon steel right-circular cylindrical tubes and frusta (Mamalis and Johnson, 1983; Mamalis et al., 1984) and tapered mild steel tubes of

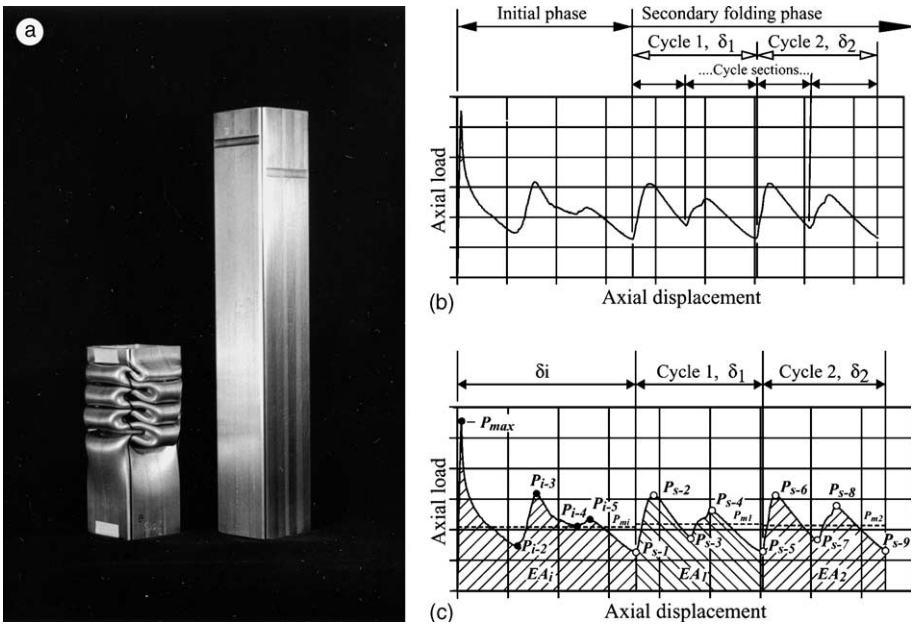

Fig. 1. Symmetric axial crush response mode—ductile metallic alloy, square box component: (a) axial crush specimen and undeformed tube; (b) curve subdivisions and (c) crush characteristics—examples.

rectangular cross-sections (Reid and Reddy, 1986b). In particular, geometric limits for quasi-static axial collapse responses have been established for right-circular cylinders of an aluminum alloy (Andrews et al., 1983) and for both static and dynamic test conditions, the transition from initial global bending collapse to axial crush response has been experimentally investigated for mild steel square and right-circular cylindrical columns (Abramowicz and Jones, 1997).

For the particular case of axial crush response, prior studies have established that there can be several modes for a given component (specific geometry and material). These modes have been extensively analyzed with respect to geometry, material parameters, and rate effects (see overview of dynamic progressive buckling in Jones, 1997). For right-circular cylindrical components, the axial crush modes include the concertina and diamond modes or a combination of the two modes (as shown in Andrews et al., 1983 for an aluminum alloy). For square tube specimens, four axial crush response modes have been identified (Abramowicz and Jones, 1984): a symmetric mode; two asymmetric mixed modes; and an extensional mode. Using experimental procedures to establish ranges for the axial crush response modes, results indicate that the symmetric axial crush mode of a mild steel square box component is associated with larger ratios of sidewall width to wall thickness (Abramowicz and Jones, 1986). It is this symmetric axial crush response mode that is the focus of the current investigation on a square box component.

1.1. Overview of axial crush response of a square box component—symmetric mode

An example of the symmetric axial crush response mode for an AISI 304 stainless steel, welded square box component tube specimen is shown in Fig. 1. The deformed specimen is next to an undeformed tube specimen in Fig. 1a and the axial load-axial displacement curve (subsequently referred to as the load–displacement curve) is shown in both Fig. 1b and c. Axial crush response is verified by both the specimen's fold appearance and the corresponding load–displacement curve.

In general, axial crush response can be considered to consist of phases or stages (Pugsley, 1960). For the current investigation, the response is divided into an "initial" phase and a "secondary" phase. The initial phase includes the pre-collapse response prior to the occurrence of the peak or maximum load, (P_{max}); the change from axial to bending load–resistance in the sidewalls; and the formation of the first few interior and exterior folds on sets of opposite sidewalls with corresponding increases and decreases in the load–displacement curve. The secondary folding phase consists of the "steady-state" fold formation process. In this phase, adjacent sidewall interactions and contacting of folds produce subsequent fold formations of "constant" wavelength along the remaining length of the specimen. This folding process produces fluctuations in the load–displacement curve. For the current investigation, a cycle in the curve (see Fig. 1b) corresponds to the formation of one exterior or one interior fold on both sets of opposite sidewalls with load magnitudes fluctuating between minimum and maximum values. Cycles can be further divided into sections. Each section represents the formation of an exterior fold on a specific set of opposite sidewalls and the corresponding formation of an interior fold on the other opposite sidewall pair.

1.1.1. Foldlines

The fold formation process has been characterized using the concept of stationary and traveling "foldlines" [for hat-section specimens—Ohkubo et al., 1974; for right-circular cylindrical polyvinyl chloride (PVC) specimens—Soden et al., 1974] or for idealized models, plastic "hinge lines" (Ohkubo et al., 1974; right-circular cylindrical and square specimens—Johnson et al., 1977; Abramowicz and Wierzbicki, 1979). For a specific fold formation process, the foldlines or hingelines represent the locations of localized plastic deformation and maximum curvature changes. For PVC tube specimens, the "foldlines" have been revealed by immersing the deformed specimens in boiling water for several seconds so that the specimens recovered their original length (right-circular cylindrical tubes—Soden et al., 1974; square tubes and frusta—Mamalis et al., 1989). Developed views of the foldlines on the original specimen geometry (right-circular cylindrical

tubes—Mallock, 1908; square tubes and square frusta—Mamalis et al., 1989), and thin sheet or paper models of hingelines (Pugsley and Macaulay, 1960; Johnson et al., 1977; Abramowicz and Wierzbicki, 1979; Abramowicz and Jones, 1984), have aided researchers in understanding the fold formation process and developing analytical models for the energy absorption aspects of axial crush response.

For square box components undergoing axial crush in the symmetric response mode, the stationary foldlines represent the centerlines for the transverse exterior and interior sidewall folds that form perpendicular to the longitudinal direction of the specimen. The traveling foldlines are associated with the corners of the box component specimen. During the crush, a traveling foldline progresses along the longitudinal axis of the specimen and crosses the same cornerline while moving back and forth between the two adjacent sidewalls corresponding to the cornerline. Ideally, at any time during the crush response, the progress of the four traveling foldlines will be at the same longitudinal position along the specimen and for the entire axial crush, foldline symmetry exists for both the stationary and the traveling foldlines, i.e., an exterior (interior) stationary foldline in a specific sidewall will occur at the same longitudinal location on the specimen as the exterior (interior) foldline in the opposite sidewall. A traveling foldline along a specific cornerline will have the same centerline path pattern as the traveling foldline along the diagonally opposite cornerline and will be the mirror image of the traveling foldlines along the adjacent cornerlines.

1.1.2. Crush characteristics

For axial crush response, investigators have used or defined "crush characteristics", also called indicators or parameters, to evaluate and compare the performance of components (Pugsley, 1960; Coppa, 1968; Magee and Thornton, 1979). Besides direct data quantities such as load magnitudes, displacements, fold wavelengths and energy absorption, other derived crush characteristics include: specific energy—maximum dissipated energy at a particular load level divided by specimen weight; energy dissipation density—maximum energy absorbed per unit volume of material; load uniformity—ratio of maximum load to average load; operating stress—ratio of average or mean load divided by the overall cross-sectional area; solidity ratio—net cross-sectional area divided by enclosed area; and structural effectiveness—specific energy divided by the specific true ultimate tensile strength. The collapse efficiencies include the geometric, stroke, strain or crush efficiency—maximum displacement divided by total length, the load efficiency—average or mean load divided by average maximum or minimum load, and the energy efficiency—maximum energy absorbed divided by the product of the maximum load magnitude times the total length.

The emphasis of the current investigation is on direct quantities attributed to the axial crush response and therefore, only the load–displacement curve crush characteristics are considered. These quantities are shown in Fig. 1c and include: the initial phase peak load, P_{max}; maximum and minimum loads, $P_{i\text{-}\#}$ or $P_{s\text{-}\#}$; mean or average loads, P_{mi} or P_{mN}; energy absorptions, EA_i or EA_N; and axial displacements, δ_i or δ_N, where the subscript 'i' refers to the initial phase, the subscript 's' refers to the secondary phase and the subscript N refers to the Nth cycle in the secondary phase. In general, an energy absorption quantity, EA, is the area under the load–displacement curve and is calculated between two displacement points and an average or mean load quantity, P_m, is equal to the energy absorption between two displacement points divided by the distance between those two points. Since variations in values for either of these two quantities may occur due to the particular points chosen for the calculation, either the displacement points (type and values) or the curve section identification, e.g., initial phase, cycle number, etc., will be specified.

1.2. Design criteria and control methods for axial crush response

1.2.1. Design criteria

Design criteria exist to provide that a box component of a specific geometry and material combination will undergo axial crush response under axial compressive loading as opposed to the other previously mentioned axial collapse modes such as elastic column buckling and bending and local elastic buckling. To

prevent elastic column instability, the length criteria from the Euler buckling formula as given in strength of materials or elastic stability textbooks (for example, Bleich, 1952) is

$$L \leqslant \frac{\pi r_g}{K_e}\sqrt{\frac{E}{\sigma_y}} \tag{1}$$

where L is the length of the undeformed column; r_g is the radius of gyration of the column (same units as L); K_e is the effective length factor; E is the modulus of elasticity; and σ_y is the yield strength of the material (same units as E). To prevent the paneling collapse of square box columns of mild and high strength steels, a compactness criteria (Mahmood and Paluszny, 1981) can be generated, assuming a plate type column under uniform axial compression and requiring that the critical elastic local buckling stress be greater than the maximum (crippling) load-carrying strength of the component. For these criteria, a steel square box component has the ability to undergo axial crush folding response under the following condition:

$$\frac{t}{b} \geqslant 0.48\sqrt{\frac{(1-v^2)\sigma_y}{E}} \tag{2}$$

where t is the wall thickness; b is the width of the "buckling" plate (same units as t); v is Poisson's ratio; E is the modulus of elasticity; and σ_y is the yield strength of the material (same units as E).

However, in practice, the criteria do not guarantee that a box component will undergo axial crush. For example, an arbitrary axial collapse, e.g., non-symmetric fold formation, may occur due to end conditions. Therefore, end constraints and collapse initiators have been employed in past research to control various aspect of the response of a specimen. The specific methods of constraint and types of initiators have depended on the geometry and material of the components as well as the research objectives.

1.2.2. Control methods

1.2.2.1. End constraints. For a test specimen under axial compression, end constraints influence the local end deformation response, and for axial crush, the fold formation process in the initial phase that subsequently provides the initial deformation required for the secondary folding phase. Past research on quasi-static and dynamic axial crush of metallic alloy components of various geometries have employed a variety of end constraint conditions including no end constraints (free at both ends), a single end constraint at the support end and no constraint at the loading or impact end (Langseth et al., 1994; Abah et al., 1998), and constraints at both ends of the specimens.

For an unconstrained or "free" end condition, interactions between the specimen and test apparatus determine the tube end deformation. Several end conditions can result: a local fold-down of specimen walls (see Meng et al., 1983 and Reid et al., 1986 for examples); a fixed condition in which specimen end walls are locally constrained from both translation and rotation across the entire cross-section; or at the fold initiation end, a mixed free-fixed end condition around the cross-section that could interfere with fold formation and cause an irregular collapse of the specimen. Therefore, for studies that require consistent boundary conditions on all of the test specimens, constraint of both ends of a specimen is a requirement.

1.2.2.2. Collapse initiators and controllers. In past investigations of ductile metallic alloys, it has been shown that collapse initiators, also called triggers, stress concentrators, or imperfections, can be used to: initiate a specific axial collapse mode; stabilize the collapse process; and for axial crush response, reduce the peak load magnitude or optimize another specific crush characteristic (Coppa, 1968; Thornton and Magee, 1977). The use of initiators also sets the start of the collapse process at a specific location on the specimen.

Initiators are based on either material or geometric modifications to the component. Examples of material modification initiators are locally annealed regions generated by concentrated heating,

or the heat-affected zone generated by a weld. Types of geometric initiators include naturally-formed and mechanically-induced modifications, structural additions or deletions on the component and for composite components, special end configurations and inserts. The initiators based on geometric modification of the component have the advantages of being visually detectable and controllable by dimension adjustment.

The naturally-formed initiators involve pre-buckling of the component past the peak load. Quasi-static prebuckling or pre-crushing of a specimen has been performed to eliminate initial peak load on honeycomb specimens (Kindervater, 1981) and to control behavior of square tubes (Langseth et al., 1994). More commonly used mechanically-induced imperfections such as local transverse indentations or crimping have been used on right-circular cylinders (Thornton and Magee, 1977) for collapse mode control and peak load reduction. Transverse full width indentations on sidewalls of square sections (Chou, 1983), indentation on right-circular cylinders and square and Z sections (Lampinen and Jeryan, 1983), and corner cutouts on square tube specimens (Abah et al., 1998) have been employed to initiate collapse and reduce the peak load. Additionally, in the structural deletion category, holes in right circular cylindrical tubes have been drilled to set the collapse initiation site, reduce the peak load, and alter the deformation mode (Gupta and Gupta, 1993). Combinations of transverse sidewall indentations and holes in square tube specimens without end constraints have been studied to control the peak load magnitude and stability of the collapse mode (Marshall and Nurick, 1998). A geometric modification to hat-section specimens by forming a flange with bend radius and stress releasing cutouts at the end of a specimen has also been studied to reduce the peak load (Tani and Funahashi, 1978).

Other physical modifications have been used to control specimen performance in both the initial and the secondary phases of axial crush. Types of these initiators-controllers include: corrugations formed in "square" tubular sections (Thornton, 1975); a series of machined circumferential grooves in right circular cylindrical tubes (Mamalis et al., 1986); drilled holes in flange bend lines, and notches cut out of flanges in flanged right circular cylinders (Grimm et al., 1988); and on hat-section specimens, partial transverse mid-sidewall dents or bulges (beading) and/or corner dents (Yamaya and Tani, 1971; Yamaguchi et al., 1985).

In summary, results of past studies have shown that for component specimens that theoretically have the ability to undergo axial crush response, collapse initiators in combination with end constraints can be used to obtain a particular axial crush mode or modify certain crush characteristics.

1.3. Configuration responses of the symmetric axial crush mode

In the current investigation, the term "configuration response" of the symmetric axial crush mode will refer to the combination of a specific fold formation process (verified by fold appearance) and the shape of the corresponding load–displacement curve. For specimens of a given component, the symmetric axial crush mode does not in general have a unique configuration response. Fig. 2 shows the fold formation and corresponding load–displacement curves for two box component specimens. For these two specimens, there is no significant difference in geometry, material, end constraint or quasi-static testing conditions and both specimens underwent symmetric axial crush mode response. However, Fig. 2a and b shows differences in both fold appearance and load–displacement curve shape and therefore, the configuration response is not the same for the two specimens.

Axial crush configuration responses of a component can differ in stationary foldline locations, traveling foldline paths (as shown in Fig. 2a and b for configurations A and B, respectively), and material performance requirements and therefore, for constant geometry and material conditions, in load magnitudes (as shown in the superimposed curves in Fig. 2c) and the energy absorption process. For studies based on overall performance quantities such as total energy absorption or "average load," the response characteristics of interest may not be significantly different if more than one configuration is obtained for component specimens. However, for studies focusing on response details such as material parameter effects

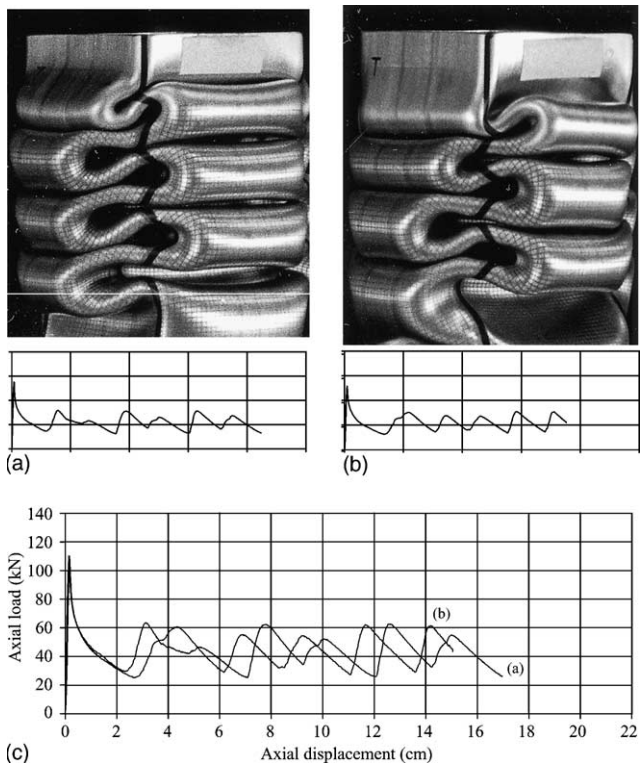

Fig. 2. Configuration responses for the symmetric axial crush mode: (a) Configuration A; (b) Configuration B and (c) superimposed load–displacement curves.

or foldline path control, the restriction of specimen response to a particular configuration may be a requirement.

1.4. Objective

Past research has established axial crush as an EA structural engineering response of ductile metallic alloys that relies on plastic deformation of a progressive fold formation process along the longitudinal axis of a component. Researchers have studied modes and overall response characteristics for a variety of geometric shapes and material combinations, derived response design criteria and predictive analytical models for crush characteristics, and investigated collapse initiation and controls and end constraint techniques. The results of these efforts have substantially contributed to engineering advancements in both crashworthiness and blast resistance. However, more research is required to fully understand and establish not only structural engineering design requirements, but also material performance criteria for these applications.

In research studies on material behavior of box components, axial crush can be used as the structural engineering response. If control techniques could restrict the axial crush response of test specimens to a particular configuration response of a mode, research could be performed to study the effects of material parameter variation on the foldline formation and energy absorption process, and to study details of material behavior such as microstructural evolution and deformation mechanisms during severe plastic deformation. However, past research has not addressed the issue of configuration response control.

The current investigation focuses on a specific symmetric axial crush mode configuration response of a thin-walled, box component using commercially-produced, welded AISI 304 stainless steel square tubing (DiPaolo, 2000). The first objective was to demonstrate the ability to consistently obtain the specific configuration response for box component specimens by using control techniques such as tube end constraints and collapse initiators. The second objective was to then use the control techniques to isolate and examine the effect of alloy composition and microstructure on the fold formation process of the specific configuration response induced in the component.

2. Experimental methodology

2.1. Box component specimens

2.1.1. Geometry

The test specimens used in the investigation were fabricated from commercially-produced, welded AISI 304 wrought austenitic stainless steel (AISI 304 SS) tubing. This form was chosen because the material is widely produced and commonly used, and has been extensively researched. The tubing is applicable to vehicular and blast-protective structural forms and is readily available from commercial suppliers in component geometries that have the ability to undergo axial crush response.

Four lengths of mill-surface finish, ornamental/structural grade tubing were purchased "off-the-shelf" from the regular stock of a commercial metallic alloy products supplier (Ryerson, 1991). Each length was approximately 6 m long (see Fig. 3a). Of the four lengths purchased, the lengths assigned the identification numbers "S1" and "S3" upon delivery from the supplier were used in this investigation. As shown in Fig. 4a, the cross-sections of the tube lengths have a square box-type geometry with rounded corners. Dimensions include nominal 50 mm × 50 mm outside dimensions, a 1.6 mm wall thickness, and an average corner inside radius of 3.6 mm. In general, the tubing is manufactured as follows (Hordijk, 2003): annealed and pickled AISI 304 stainless steel strip coils (1.6 mm by 1.2 m wide) are obtained from a steelmill; in a continuous process, the material is fed through a slitter to cut the strip into approximately 198 mm widths that are cold formed in consecutive passes on a continuous mill into round tube (approximate diameter of 63 mm) and longitudinally welded utilizing the GTAW (TIG) welding process; and in several more consecutive passes, the tubing is first "calibrated" in sizing passes, i.e., squeezed to round size within ±0.30 mm and then, cold-formed in shaping passes by sets of rollers with a ground rollface of increasingly higher radius into the square section with the weld seam positioned near the center of a sidewall (see Fig. 4a). Finally, the tubing is cut into appropriate lengths and shipped to distributors. It should be noted that as the square tubing is formed, mechanical properties are modified by cold-working and residual stresses are induced in the tube material. The tube is not annealed during or after the manufacturing process.

2.1.2. Sectioning of the tube lengths and tube specimen numbering systems

From prior axial crush testing of specimens with similar geometry and material, it had been determined that a tube specimen length of 30.5 cm was adequate to obtain at least two full fold cycles in the secondary folding phase of several symmetric axial crush mode configuration responses without the tube end constraint conditions adversely affecting the secondary phase fold formation process. This 30.5 cm length was used as the axial crush tube specimen length in the length cutting sequence shown in Fig. 3a. For both S1 and S3 samples, one end of the tube was arbitrarily chosen as the "start" end for the cutting of tube specimens. An initial cutting and a subsequent cutting resulted in nineteen 30.5 cm tube specimens and four miscellaneous tube pieces of lengths less than 10.0 cm. All sectioning was performed using an abrasive chop saw (cutoff saw). Cutting lines were made as square as possible to the longitudinal axis of the 6 m tube length. All tube specimen ends were deburred, but not milled.

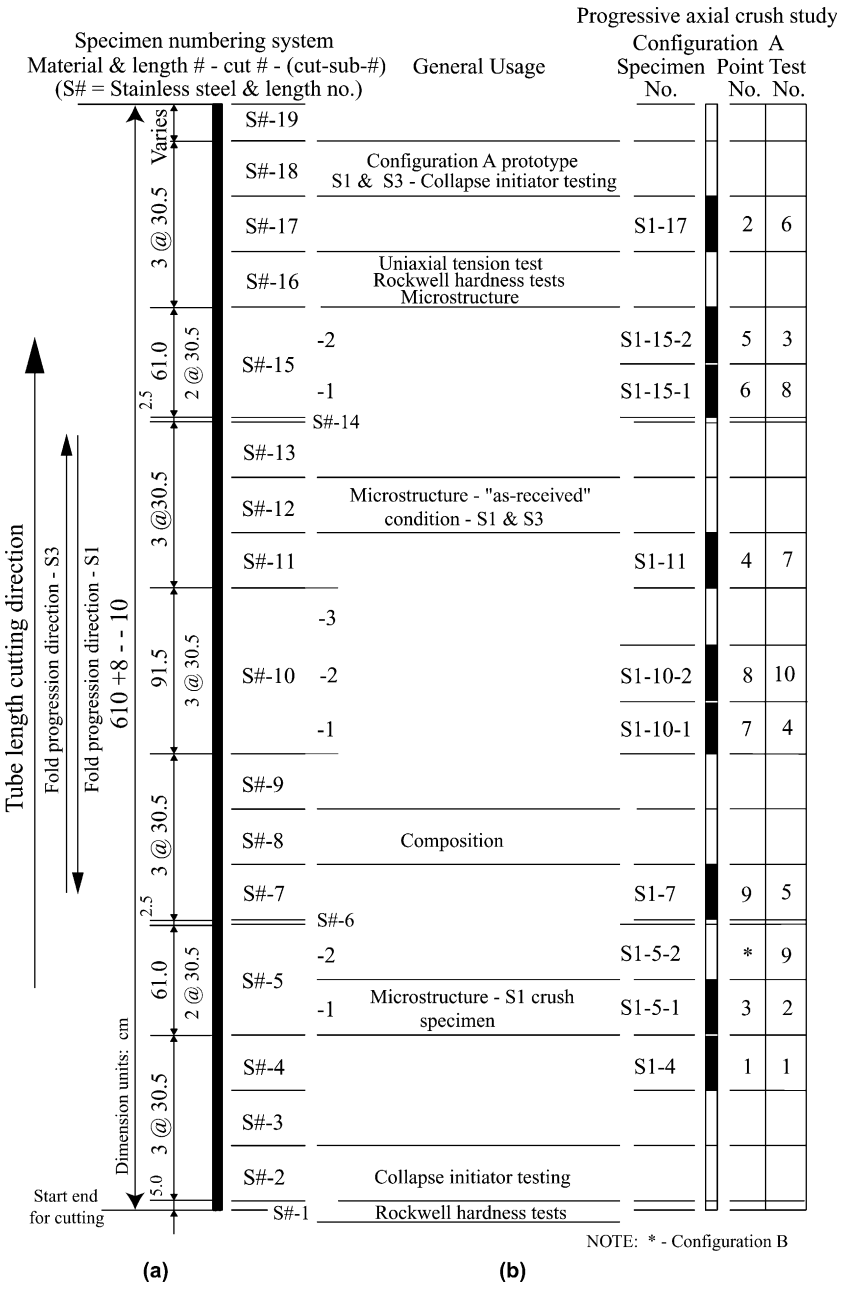

Fig. 3. Tube length cutting diagram, specimen numbering system and usage: (a) tube length cutting and tube specimen numbers and (b) usage diagram.

A specimen numbering system (Fig. 3a) was developed to track the original tube length location for a tube specimen or piece. The specimen number was of the form: S#, for # = 1 or 3-initial tube length cut number (cut-sub-number, if applicable). Each tube specimen had its specimen number engraved at two specific locations. The orientation of the numbers indicated the tube length cutting direction on the tube

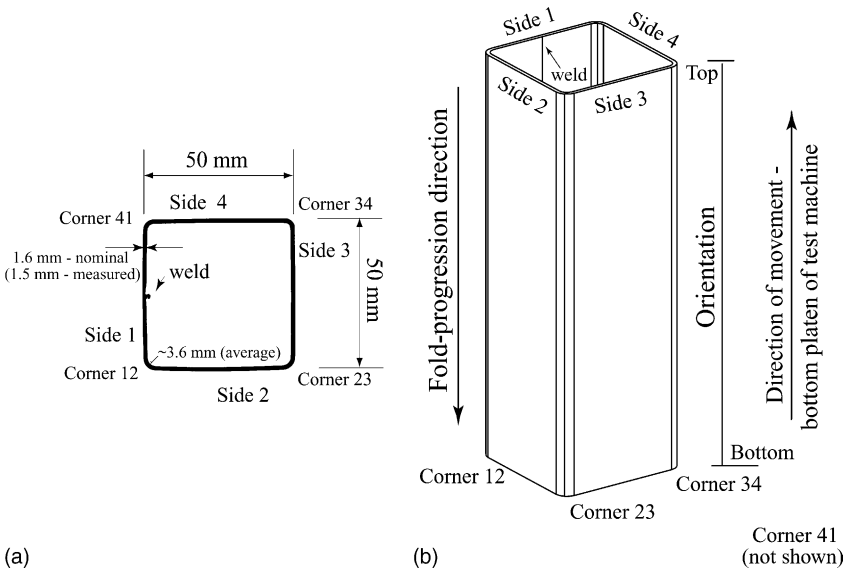

Fig. 4. Tube geometry and side and corner numbering systems: (a) typical cross-section geometry and (b) tube specimen orientation.

specimen. Using the cutting direction, a sidewall and corner numbering system as shown in Fig. 4b was developed to locate and identify corners and orient any material point on a specimen along the original tube length and around the tube cross-section.

For several tube specimens, outer dimensions were measured and recorded and corner radii were calculated from cross-section images. For every tube specimen, wall thicknesses on all four sides were measured and cross-section outline tracings of the ends were superimposed. The measurements and tracings indicated no significant difference in outer perimeter shape and dimensions and in wall thickness between tube specimens. Therefore, tube specimens from both the S1 and S3 lengths had essentially constant geometry.

2.1.3. Material

Type 304 SS is a wrought austenitic stainless steel, alloyed with 18% chromium and 8% nickel. It is noted for high strength, ductility and strain hardening capability and exceptional toughness. It is also considered "meta-stable" because it may have the ability to undergo a strain-induced martensitic transformation when subjected to severe plastic deformation at temperatures around 20 °C (room temperature) (Angel, 1954; Gray et al., 1985; Griffiths and Wright, 1969). If the transformation can occur, the strength behavior, e.g., strain-hardening and stress–strain curve shape, in a given stress/strain state is primarily derived from the mechanical response of the austenite, the transformation from austenite to martensite, and the mechanical response of the product martensite. The occurrence and degree of the transformation depends not only on the composition, grain size, grain orientation, and temperature during deformation, but also on the stress/strain state and strain magnitude, rate and path. For stress/strain states, the order of decreasing occurrence is: balanced biaxial tension, uniaxial tension, compression, and torsion (Powell et al., 1958; Hecker et al., 1982).

For AISI 304 stainless steel, two types of strain-induced martensite can form: a ferromagnetic body-centered cubic α' phase and a non-ferromagnetic hexagonal close-packed ε phase. In the annealed state, the material is generally non-magnetic and therefore, after severe plastic deformation, a positive response to a small magnet would indicate that α'-martensite had formed in the area and that the martensitic transfor-

mation had occurred. No response was felt when a small, hand-held magnet was moved over the surfaces of S1 and S3 tube specimens in the "as-received" condition.

2.1.3.1. Composition. Compositional analysis (Foreman, 1999) of material from tube specimens S1-8 and S3-8 are given in Fig. 5a. Ranges or maximum allowed weight percents for elements from ASTM Designation A 666-99 (ASTM, 2000) for AISI 304 SS are also given in Fig. 5a.

A comparison of the values indicates that the material for the S1and S3 tube lengths meets the composition requirements for commercial AISI 304 stainless steel; however, variations in composition exist between the S1 and S3 tube length materials. Specifically, the analysis indicates a slightly higher carbon content for the S3 material.

2.1.3.2. Microstructure. Visual observation of the microstructures for the S1 and S3 tubes was performed on material from as-received specimens S1-12, S3-12, S1-16 and S3-16 and also from S1-5-1 after it was axially crushed. Material was sectioned from the tube specimens using hacksaws and jeweler's saws, mounted in castable (cold) Epoxide resin and hardener compound (Buehler, 1999), ground and polished using water-based diamond suspensions through the 0.1 μm stage, and etched using glyceregia. Optical microscopy was performed using a LECO 300 Metallograph with Xenon light source and the crossed-polarized filters. For the different locations along the tube length and around the cross-section, through-thickness, transverse

	Element (wt %)							
	Cr	Ni	C	N	Si	Mn	P	S
ASTM Standard for AISI Designation Type 304 Stainless Steel								
Min.	18.00	8.00						
Max.	20.00	10.50	0.08	0.10	0.75	2.00	0.045	0.030
Commercial laboratory* composition analysis - S1 & S3 materials								
S1	18.26	8.16	0.045	0.053	0.45	1.69	0.025	0.014
S3	18.66	8.05	0.053	0.052	0.45	1.89	0.024	0.011

Balance - Fe + others

* Reference: Foreman, 1999

(a)

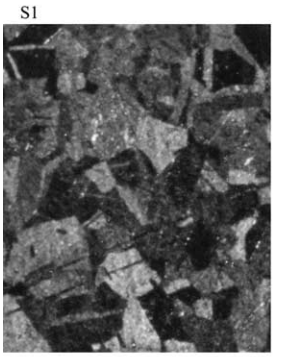

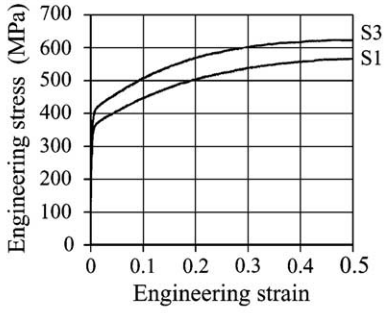

330	0.2% offset yield stress (MPa)	370
570	Ultimate strength (MPa)	630

(b)

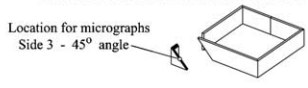

Fig. 5. "As-received" material—S1 and S3 tube lengths: (a) alloy compositions and (b) microstructures—relative grain size and uniaxial tension test curves and strengths.

and longitudinal grain sizes and the character of the microstructure were found to be consistent in the S1 tube length and also in the S3 tube length. However, as shown in the micrographs in Fig. 5b, the grain sizes in the S3 material were significantly smaller than those in the S1 material.

2.1.3.3. Mechanical properties. To obtain material strength and ductility data, uniaxial tension tests were performed. Sheet tensile specimens (200 mm in length) from the middle area of side 3 (sidewall opposite the weld) were obtained from tube specimens S1-16 and S3-16 using an abrasive cutoff saw with water coolant. The longitudinal axis of each tension specimen was parallel with the longitudinal axis of the tube specimen. Uniaxial tension tests (ASTM, 1997) at 20 °C were performed using an MTS universal testing machine (MTS Load Frame 100/200 kN—University of California at Berkeley (UCB)), a 50 mm gage length extensometer and a computer-based data acquisition system. Testing was performed in the displacement control mode with the machine ram (bottom platen) speed set at approximately 2.5 mm/min. The engineering stress–engineering strain curves are shown in Fig. 5b. The 0.2% offset yield stresses were 330 MPa for the S1 material and 370 MPa for the S3 material. The ultimate tensile strengths were 570 and 630 MPa for the S1 material and the S3 material, respectively. For both materials, the tensile strength values are well above the minimum required ASTM Designation E 8-96a (ASTM, 1997) 0.2% offset yield stress of 205 MPa and ultimate strength of 515 MPa for AISI 304 SS in the annealed condition. A small, hand-held magnet was pulled across the tested uniaxial tension specimens and for both the S1 and S3 specimens, a positive attraction of the specimens to the magnet occurred in the uniform elongation and necked sections, but not in the transition and grip sections. Therefore, the results of the quasi-static, room temperature, uniaxial tension tests indicated that α'-martensite had formed and both the S1 and S3 materials have the ability to undergo the martensitic transformation.

Hardness testing was performed using a Rockwell Hardness Tester (Model 3JR-No. 4147, Wilson Mechanical Instrument Division at UCB) on material from tube specimens S#-1 and S#-16, for $\# = 1$ and 3, at multiple locations around the cross-section. Average RHB values of 95 for the outside surface and 93 for the inside surface were obtained for the S1 material and average RHB values of 98 for the outside surface and 96 for the inside surface were obtained for the S3 material.

The results of the composition analyses and uniaxial tension tests indicate that both the S1 and the S3 samples meet the standard requirements for commercial grade AISI 304 SS. Because the fabrication process involved cold-forming and welding, there is expected variation in material properties around the cross-sections for either tube length, but this cross-sectional variation is consistent along the length as indicated by microstructure appearance and hardness readings. Therefore, S1 and S3 tube specimens have "constant" geometry and although material can be considered "constant" along the length for tube specimens from the same tubing length, the S3 material is higher in strength than the S1 material.

Finally, a check on the elastic global buckling and the compactness criteria for the geometry-material combinations of the S1 and S3 tubing was performed. Assuming a simply supported column such that $K_e = 1$ and using Eq. (1), the tube specimen length of 30.5 cm is less than the maximum length, L, of 140 cm to prevent elastic column instability. For the compactness criteria, the t/b ratio of 0.030 is greater than the required minimum value of 0.021 as calculated from Eq. (2) for the higher strength S3 material. Therefore, when axially loaded in compression, the S1 and S3 tube specimens without collapse initiators to reduce the peak load will not globally or locally buckle and have the ability to undergo axial crush response.

2.2. Axial crush configuration response control techniques

2.2.1. End constraint—end caps

For axial crush testing of several specimens of a given component, end constraints are required to ensure consistent boundary conditions. In past research, types of end constraints for box and hat-section com-

ponents have included end plates attached by welding or spot-welding to the specimens (Yamaya and Tani, 1971; Ohkubo et al., 1974; Chou, 1983; Lampinen and Jeryan, 1983; Yamaguchi et al., 1985; Wong et al., 1997) and grooved plates (Toda et al., 1976; DiPaolo, 1992). Unlike grooved plates, welded plates require additional specimen preparation time and cost and the welding process can cause distortions and localized microstructural changes in the specimens. Therefore, groove plates were chosen for the current investigation.

The removable, grooved end cap plates (DiPaolo, 2000) that were used for tube end constraint are shown on a specimen during testing in Fig. 6a and in detail in Fig. 6c. Each of the end caps was machined from a 100 mm diameter and 25 mm thick circular piece of AISI 4140 (Cr–Mo alloy) steel. After machining, caps were heat-treated and ground flat. The ability to reuse the caps for components with the same nominal cross-sectional dimensions required that the width of the grooves allowed for manufacturing tolerances on the tube specimen's cross-section. Because the grooves were always slightly wider than a specimen's outside width and slightly narrower than the specimen's inside width, the end cap method could not provide full fixity on the specimen ends. However, the end cap grooves provided local support to specimen sidewall ends and consistent end conditions from specimen to specimen.

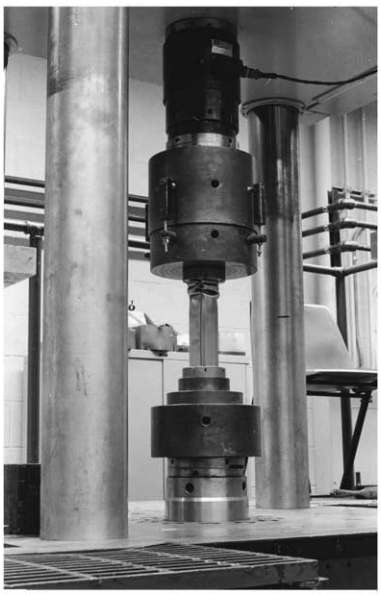

QUASI-STATIC TESTING

MTS universal testing machine
- 1350 kN capacity
- cross-head speed =2.5 mm/min
- displacement control
Temperature - 20°C

(a)

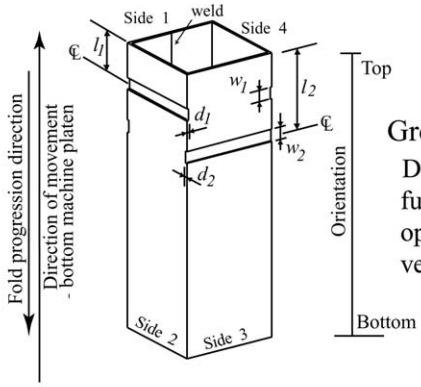

Groove design:
Double set of machined full width grooves in opposite sidewalls with vertical offset

Groove dimensions:

		Upper set - "set 1"		Lower set - "set 2"		
			S1	S3		S1	S3
	width (mm)	w_1	6.4	6.4	w_2	6.4	6.4
	depth (mm)	d_1	0.23	0.25	d_2	0.18	0.20
(b)	distance from top end of tube (mm)	l_1	21.6	21.6	l_2	44.5	44.5

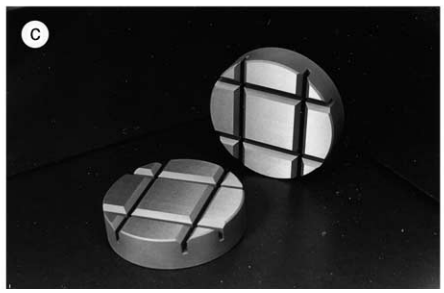

Fig. 6. Experimental test set-up and controls: (a) test machine set-up; (b) collapse initiator geometry and (c) grooved end cap set for tube end constraints.

2.2.2. Collapse initiators—machined sidewall grooves

Collapse initiators were used in the investigation to set the axial locations for the initial inward collapse of all four sidewalls for a tube specimen, to control the fold formation in the initial phase of the crush, and to establish the specific deformation conditions required for the natural secondary fold formation phase of a specific axial crush configuration response. Machined grooves in the sidewalls at one end of a tube specimen served as collapse initiators. This geometric modification was chosen because of the dimensional control and repeatability of the machining process.

The collapse initiators specifically consisted of a double set of transverse, full sidewall width, machined grooves in opposite sidewalls with a vertical offset for groove pairs in adjacent sidewalls. An undeformed tube specimen with grooves is shown in Fig. 1a. The geometry and dimensions for the groove design are given in Fig. 6b. The design was developed in preliminary collapse initiator testing (DiPaolo, 2000) of prototype specimens from the S1–S4 tube lengths. The basic requirement for the design was to force sidewall movement inward at the same specific locations for each pair of opposite sidewalls, and to control the initial phase fold formation of a configuration without disrupting the deformations required for the secondary fold formation phase for that configuration. The location and spacing of the grooves was based on the geometry of the natural wavelength in the initial fold formation phase of specimens that had been tested with end caps but without initiators and that had undergone configuration responses similar to the Configuration A response shown in Fig. 2a. The width of the grooves was set at slightly less than the curve length of the corresponding inward fold on an unmodified specimen for the configuration response and the groove depth of 10–15% of the wall thickness was used to induce localized bending moments in the sidewalls without disrupting the fold formation process. The grooves were produced using an end mill cutter in a milling machine and by performing two to three passes per groove to obtain the specified depth at midwall. No blending of the grooves to the surface was done. The grooves were machined at the "end of cutting" end for S1 tube specimens and at the "start of cutting" end for S3 tube specimens.

2.2.3. Test setup

All axial crush testing was quasi-static at 20 °C using a 1350 kN capacity MTS universal testing machine with computer control and data acquisition systems (MTS Load Frame 1000/2000 kN—UCB). The testing mode was displacement control with the bottom platen of the machine being moved vertically upward to load the tube specimens in compression. The ram speed was 2.5 mm/min. For each specimen, masking tape shims were placed on the sidewall centers on both ends of a tube specimen in a symmetric manner (equal number of layers for opposite sidewalls). Shims were placed on the outside for sidewalls 2 and 4 and on the inside for sidewalls 1 and 3 to ensure centering of the specimen in the end cap grooves. Each specimen with end caps was placed vertically in the testing machine with the specimen's collapse initiator grooves nearest the top platen. Therefore, the folding direction in the specimen was downward and opposite to the bottom platen's upward movement. The test set-up is shown in Fig. 6a. Computer data included time, load (load cell digital resolution of ±0.7 kN), and displacement (linear-variable differential transformer, LVDT) at a recording rate of approximately one data point per second. The load–displacement curves were generated using the computer data smoothed by three-point averaging.

3. Experimental investigation

For the experimental investigation, a progressive axial crush study was performed to demonstrate that for constant test specimen geometry and material, a specific configuration response of the symmetric axial crush mode could be obtained by using experimental control methods and secondly, an alloy and microstructure study was performed using the specimens from two tubing lengths to isolate material effects for the same specific symmetric axial crush configuration response.

3.1. Progressive axial crush study

In past research, general analyses of the deformation stages in the fold formation process with respect to points on the load–displacement curves had been performed for the symmetric axial crush mode of impacted mild steel box columns (Wierzbicki et al., 1978), for quasi-statically tested, aluminum alloy box columns (DiPaolo, 1992), and for the diamond axial crush mode of quasi-statically tested right-circular cylindrical tubes of alloys of brass, copper and aluminum (Singace, 1999). However, the studies did not demonstrate that the response was limited to a single configuration response for the axial crush mode. For the experimental investigation, a progressive axial crush study was used to test the capability of simple experimental techniques of end caps and grooved collapse initiators to restrict a component's symmetric axial crush response to a specific configuration.

In the current progressive axial crush study, original geometry, material, testing conditions, and test specimen end constraints are held constant and a single axial crush configuration response is to be obtained for all specimens. The general procedure for the study consists of selecting several displacement points on the load–displacement curve of a prototype test specimen for the configuration, and for each curve point, one test specimen is axially crushed to the curve point displacement. The single axial crush configuration response is verified by comparing both fold appearance and load–displacement curve shapes for the specimens. If good agreement results, it can be concluded that consistent configuration response is obtained and the set of specimens represents the permanent deformation of the fold formation process for the configuration. The crush characteristics such as load magnitudes, displacements, and energy absorption in the initial phase and for cycles in the secondary phase of the configuration are also established for the material.

3.1.1. Symmetric axial crush mode configuration for the progressive axial crush study

In prior test studies on collapse initiator designs (DiPaolo, 2000), the symmetric axial crush mode Configuration A response (see Fig. 2a) was established experimentally by the response of the prototype specimen S1-18. The fold formation and load–displacement curve for this configuration are shown in Fig. 7 and were also used for the symmetric axial crush response example in Fig. 1. Because the end caps do not provide total fixity to the tube ends, some variation in the load–displacement curve in the initial phase of the axial crush response is to be expected from specimen to specimen. Therefore, the curve points for the study are selected from the second cycle in the secondary folding phase. The initial phase and the first cycle of the secondary folding phase are used to verify that the specimens underwent the axial crush Configuration A response. The nine points for the study are shown in Fig. 7b and include the two maximum loads,

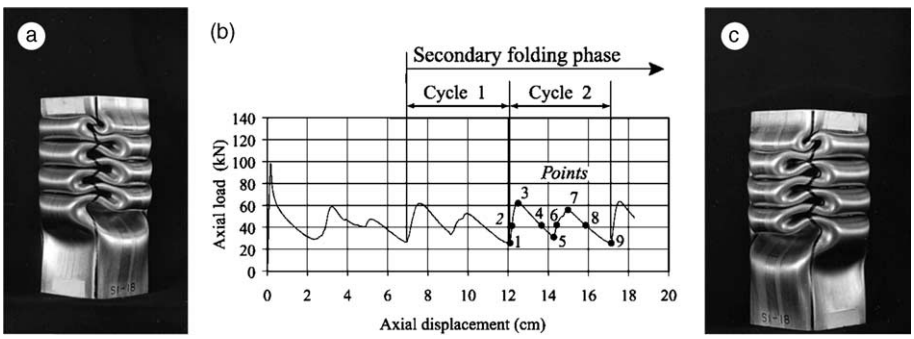

Fig. 7. Configuration A response—prototype specimen S1-18 Progressive axial crush study curve test points: (a) fold formation—corner 41; (b) load–displacement curve and (c) fold formation—corner 12.

the three minimum loads, and four intermediate points at a load of 44.5 kN (approximate expected mean load magnitude for the cycle).

3.1.2. Testing procedures

Ten 30.5 cm S1 tube specimens were selected and prepared for testing. This included one specimen for each of the selected curve points and one "extra" specimen. The locations of the specimens along the original "S1" tube length are shown in Fig. 3b. Prior to testing, a transverse dent was observed on a sidewall of specimen S1-10-2. This specimen was set aside as the "extra" test specimen. The remaining nine specimens were placed in a large box and randomly selected for testing to avoid correlation of a specimen's tube length location with its test sequence number. The testing order of the curve points was points 1, 3, 5, 7, and 9 and then points 2, 4, 6, and 8. The curve point test order was set to obtain fold formation configurations for the minimum and maximum load points before the intermediate load points.

Testing was performed over the course of two days. The curve point numbers and test sequence numbers for the tube specimens are shown with respect to the tube length locations in Fig. 3b. On the second day of testing, although specimen S1-5-2 underwent symmetric axial crush mode response, the fold appearance did not match that of the Configuration A prototype specimen S1-18. To obtain the deformation configuration for curve point 8, specimen S1-10-2, with the transverse dent, was tested. For this specimen, the machined grooves initiated the collapse of the specimen and folding proceeded similar to specimen S1-18 until the traveling foldlines reached the area containing the dent. The location of the dent in the sidewall coincided with the location for a stationary inward fold occurring in the last half of cycle 1 in the secondary folding phase. The overall fold process and appearance of the mode was not disrupted. However, the curve data for the specimen was affected because the dent acted in the secondary folding phase as a physical modification to the specimen's geometry and exclusion of the use of the data for this specimen is as noted below.

3.1.3. Results

A total of eleven box component specimens from a single "S1" length of commercial AISI 304 SS welded tubing, i.e., constant geometry and material, had been axially compressed using end caps for tube end constraint and machined groove collapse initiators for configuration response control. This included a prototype specimen, S1-18, that established the Configuration A response for the symmetric axial crush mode and ten specimens in the progressive axial crush study. For all ten specimens in the study, collapse initiated at the machined grooves; fold appearance and curve shapes indicated that response was the symmetric axial crush mode response. Fold appearance of only one specimen differed from the configuration response of the prototype specimen. This may be attributable to the end cap groove width tolerance and/or the dimensions such as location, depth, etc., of the collapse initiator grooves. However, nine of the ten specimens in the study had fold formation similar to that of the prototype specimen S1-18. For these specimens, fold formation, load–displacement curve shapes and crush characteristics were evaluated.

3.1.3.1. Fold formation process. Two views of the nine progressive axial crush study specimens are shown in Fig. 8. The fold formation is consistent from specimen to specimen and matches that of the prototype specimen S1-18 shown in Fig. 7. For the "stationary" foldline deformations, three specimens were chosen for sectioning: S1-4, S1-5-1, and S1-15-2. These specimens represent curve points: 1, 3, and 5, respectively, as shown in Fig. 9a. Sectioning was performed along longitudinal lines to obtain and compare mid-sidewall permanent deformation profiles from sides 2 and 3. The sectioning lines for the profiles are shown in Fig. 9b. Sectioning was performed using a hacksaw or when sawing became difficult due to residual stress release, a jeweler's saw. No lubrication was used; however, slow sawing speed was maintained to prevent overheating of the material in critical areas and all cut lines were deburred. The mid-sidewall fold profiles for the three specimens are shown in Fig. 9c. The deformations in the profiles represent fold formation and some residual stress release displacements; however, both sets of profiles again show very consistent

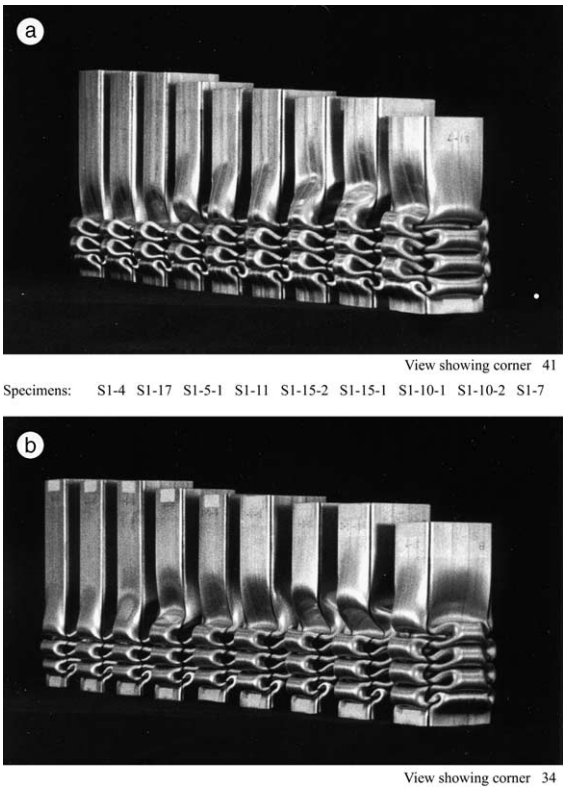

Fig. 8. Progressive axial crush study—secondary folding phase—cycle 2.

deformations in the specimens through the portion of the axial crush common to the three specimens, i.e., the initial phase and cycle 1 of the secondary folding phase.

3.1.3.2. Load–displacement curves. The load–displacement curves for the nine curve point specimens are superimposed in Fig. 10a. The figure shows that curve shape is very similar for all specimens and that the sidewall dent in specimen S1-10-2 had the effect of shifting the load–displacement curve to the left and reducing both load magnitudes and energy absorption as folding progressed through the dent area. The load–displacement curve shapes in the secondary folding phase were evaluated by separating the curves into cycle sections at the minimum loads. Fig. 10b presents the superimposed load–displacement cycle sections. For cycle 1, the sections were horizontally shifted and centered because all nine specimens were crushed through this cycle. The cycle 2 sections were horizontally shifted and anchored at the respective first minimum load points. With the exception of the curve for the specimen with the sidewall dent, the curve shapes match on a point-to-point basis. In general, the consistent fold appearance, mid-sidewall profiles, and load–displacement curve shapes indicate that the nine curve point specimens underwent the Configuration A response of the prototype specimen S1-18.

3.1.3.3. Crush characteristics analysis. To evaluate the response, crush characteristics were analyzed for the initial phase and cycle 1 of the secondary folding phase. The test data included the prototype specimen, S1-18 and eight of the nine progressive axial crush configuration specimens. The test data for specimen S1-10-2 was not included in the analysis because the transverse sidewall dent interfered with the natural fold

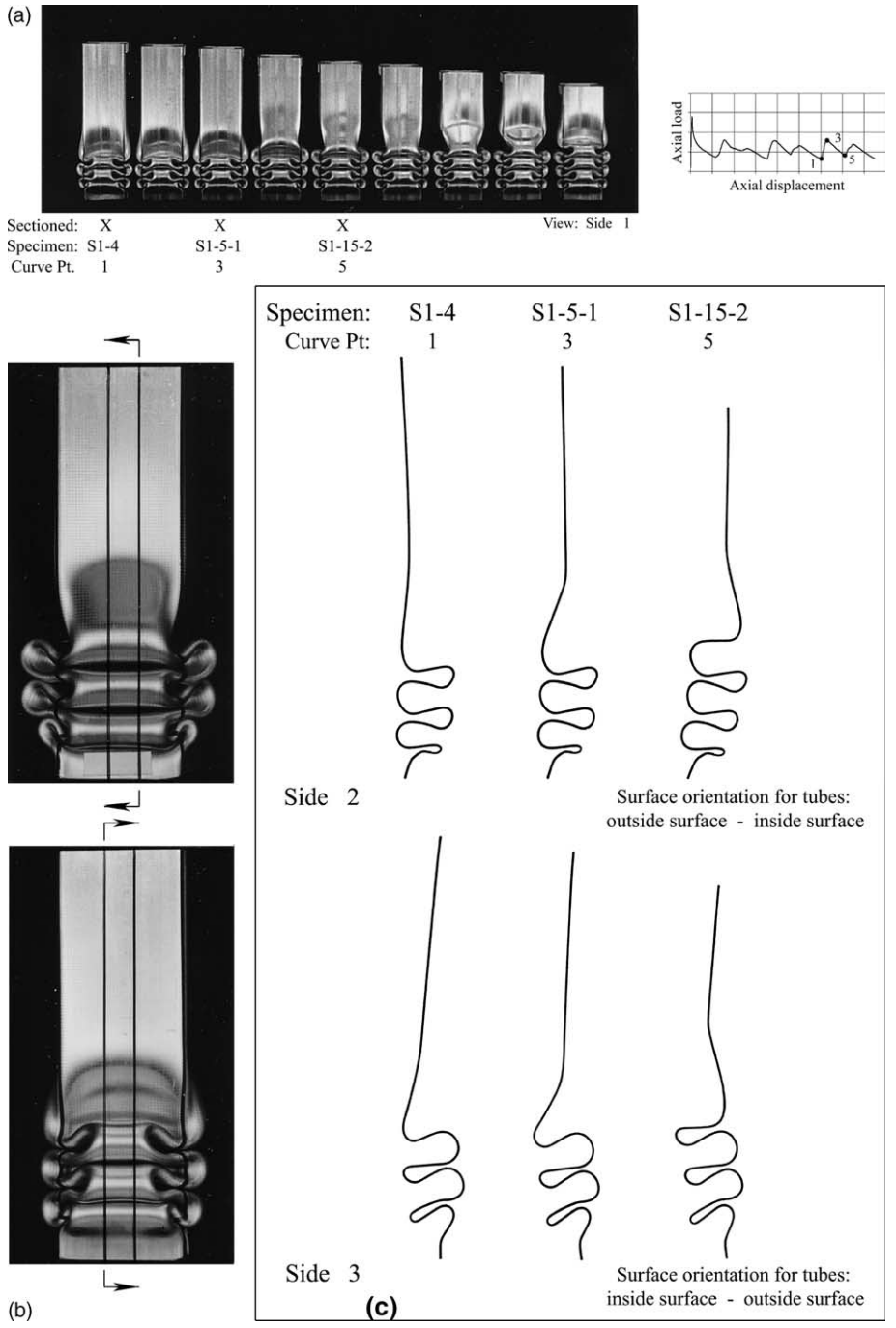

Fig. 9. Mid-sidewall fold profiles: (a) fold formation specimens for sectioning; (b) sectioning lines in sides 2 and 3 using specimen S1-5-1 and (c) profiles.

formation process in the secondary folding phase. The analysis was performed by calculating the percent differences using an average value basis and is presented in Table 1 for the initial phase and in Table 2 for

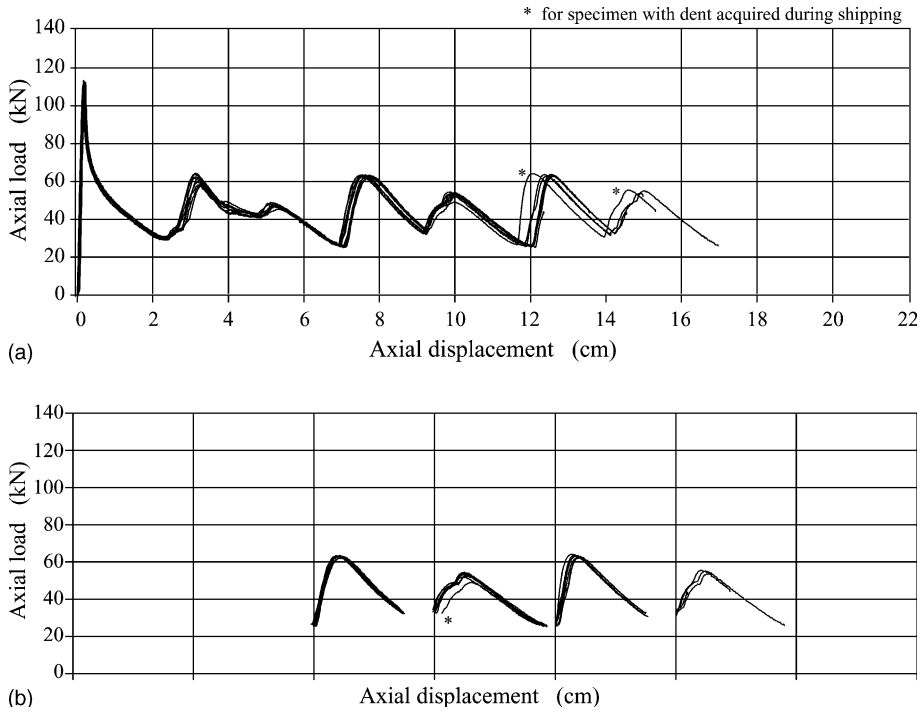

Fig. 10. Nine progressive axial crush study specimens—load–displacement curves: (a) superimposed load–displacement curves and (b) superimposed load–displacement cycle sections.

Table 1
Crush characteristics—initial folding phase, progressive axial crush study—S1 specimens

Specimen number	Curve pt.	Load (kN)					P_{mi} (kN)	δ_i (cm)	EA_i (kN cm)
		P_{max}	P_{i-2}	P_{i-3}	P_{i-4}	P_{i-5}			
Progressive axial crush study									
S1-4	Pt. 1	113	30.0	65.2	41.7	46.9	43.0	7.12	317
S1-17	Pt. 2	107	28.7	62.5	40.4	45.6	41.8	7.05	308
S1-5-1	Pt. 3	115	30.0	60.0	41.0	47.6	42.0	6.90	302
S1-11	Pt. 4	111	29.9	62.5	41.7	48.2	42.8	7.08	314
S1-15-2	Pt. 5	109	29.3	58.6	41.7	48.2	41.6	6.92	300
S1-15-1	Pt. 6	113	30.0	58.6	41.7	48.9	42.4	6.93	305
S1-10-1	Pt. 7	115	28.7	58.6	41.7	49.5	42.3	6.89	303
S1-10-2	Pt. 8	Structural damage on specimen					Transverse dent		
S1-7	Pt. 9	111	29.3	64.5	41.7	46.9	42.7	7.07	314
Basic axial crush mode—prototype specimen S1-18									
S1-18	–	99	28.7	59.3	39.8	47.6	41.3	6.96	299
Maximum percent difference (average value basis)									
		10	2	7	4	4	2	2	3

cycle 1 of the secondary folding phase. The characteristics that were included in the analysis are shown in Fig. 1c. For the initial phase, maximum percent differences were less than or equal to 10% for peak load, 7% for maximum loads, 4% for minimum loads, and 3% for mean load, cycle displacement, and energy

Table 2
Crush characteristics—secondary folding phase, progressive axial crush study—S1 specimens

Specimen number	Curve pt.	Cycle no.	Load (kN)					P_{m1} (kN)	δ_1 (cm)	EA_1 (kN cm)
			P_{s-1}	P_{s-2}	P_{s-3}	P_{s-4}	P_{s-5}			
Progressive axial crush study										
S1-4	Pt. 1	1	24.8	63.2	34.5	53.4	26.1	45.2	4.83	219
S1-17	Pt. 2	1	24.8	62.6	33.2	52.8	24.8	43.5	5.08	221
S1-5-1	Pt. 3	1	26.1	63.9	31.3	54.1	24.8	44.1	5.08	224
S1-11	Pt. 4	1	25.4	63.9	33.9	54.7	26.1	44.8	4.97	223
S1-15-2	Pt. 5	1	26.1	63.2	33.2	53.4	25.4	44.0	4.98	219
S1-15-1	Pt. 6	1	26.1	63.9	32.6	54.1	25.4	44.1	5.13	227
S1-10-1	Pt. 7	1	26.1	63.9	31.9	55.4	26.7	44.6	4.94	221
S1-10-2	Pt. 8	1	Structural damage on specimen					Transverse dent		
S1-7	Pt. 9	1	24.8	63.2	33.9	52.8	25.4	44.3	4.92	218
Basic axial crush mode—prototype specimen S1-18										
S1-18	–	1	26.1	62.6	33.2	53.4	24.8	43.7	5.07	222
Maximum percent difference (average value basis)			3	2	6	3	5	2	3	2

absorption. For the secondary phase—cycle 1 crush characteristics, percent differences were less than or equal to 3% for maximum loads, 6% for minimum loads and 3% for mean load, displacement, and energy absorption. The higher percent differences for the peak and maximum load magnitudes in the initial phase were expected due to the fact that the end caps cannot provide total fixity to the tube specimen ends. In general, the results of the progressive axial crush study showed that control methods can be used to obtain consistent performance from specimen to specimen on a point-to-point basis during the different phases of the fold formation process of a specific symmetric axial crush configuration response. Further investigations are required to study variation in crush characteristics for different symmetric axial crush mode configurations.

3.2. Alloy composition and microstructure study

3.2.1. Background

Past investigations have been performed to study the effects of alloying and process parameters on the axial crush response of metallic alloy components. A change in response mode from ductile fold formation to fracture has been reported for right-circular cylindrical tube specimens of different alloy-aging treatment combinations of AA6061-T6 and AA2024-T4 aluminum alloys (Magee and Thornton, 1979) and with different cold-worked and heat-treatment quenching processes involving dual phase steel (Thornton, 1979) and for square specimens with different processing and heat treatments of a 6XXX aluminum alloy (Logan et al., 1993). Similar response mode changes have also been observed for dynamically tested AA6082 box sections in the T4 and T6 heat treatment conditions (McGregor et al., 1993). Furthermore, for both quasi-static and dynamic testing, it had been demonstrated that material and processing changes can also be used to modify the type of mode response and crush characteristic magnitudes while retaining the ductile fold formation response of axial crush (VanKuren and Scott, 1978; Gupta and Gupta, 1993; Logan et al., 1993; Langseth et al., 1994). However, the crush characteristics used for these comparisons were limited to the peak load that occurs at the beginning of the crush and overall crush characteristics such as mean load or total energy absorption. In these studies, the axial crush mode was not restricted to a specific configuration response and no comparisons could be performed on load–displacement curve shapes or secondary folding

phase crush characteristics. The purpose of the second part of the current investigation was to isolate the effect of material parameters such as alloy composition and microstructure on the secondary folding phase of the symmetric axial crush Configuration A response.

3.2.2. Test specimens and procedure

For the second study of this investigation, test specimen geometry, end constraint, collapse initiator design and testing conditions were held constant. One specimen from each of the S1 and S3 lengths was used: specimen S1-7 (point 9—progressive axial crush study) that was compressed to the end of the second cycle in the secondary folding phase and specimen S3-18 that was compressed partially into the third cycle of the secondary folding phase.

3.2.3. Results

Photographs of the fold deformations and load–displacement curves for specimens S1-7 and S3-18 are shown in Fig. 11a and b, respectively. The similar fold appearance and overall shape of the load–displacement curves indicate that both specimens underwent Configuration A response.

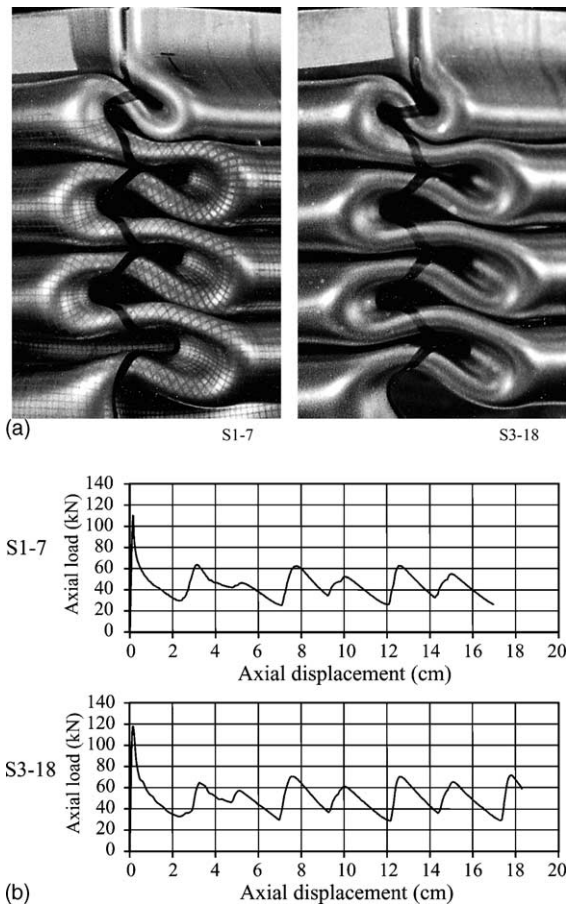

Fig. 11. Alloy composition and microstructure study, axial crush Configuration A response—S1 and S3 specimens: (a) fold formations and (b) load–displacement curves.

The secondary folding phase cycle sections of the load–displacement curves were horizontally shifted, centered and superimposed for specimens S1-7 and S3-18 as shown in Fig. 12a. The plot of the superimposed cycle sections from the S1 specimens in the first part of the investigation (dented specimen curve not included) is shown to the same scale in Fig. 12b. Since all specimens have "constant" geometry, control methods, test conditions and configuration response, a comparison of the two plots indicates that the variation in load–displacement curves is minimal for the "constant" material S1 specimens and that the differences between the curves for the S1 and S3 specimens are a result of material parameters.

In Fig. 12a, all of the S3-18 curve sections have higher load magnitudes on a point-to-point basis, increased energy absorption, and a slightly broader shape than the corresponding S1-7 specimen curve sections. An analysis of the secondary folding phase crush characteristics was performed for the S1-7 and S3-18 specimens and is presented in Table 3. The minimum percent increases for the S3 values with respect to the S1 values for the maximum loads, the minimum loads, and the mean load and the energy absorption quantities are 12%, 8%, 12%, and 18%, respectively. The percent increase of the maximum loads is consistent with the higher strength of the S3 material. The S3-18 cycle displacements are 4% larger than the S1-7 cycle displacements.

Response to a small hand-held magnet placed over the outside surfaces of the S1 and the S3-18 axial crush specimens indicated that the martensitic transformation had occurred at corner locations and along the traveling foldlines for specimens from both materials. No response was apparent on the mid-sidewall fold areas. Further investigation is required to detail and use the locations of both the α'-martensite and the

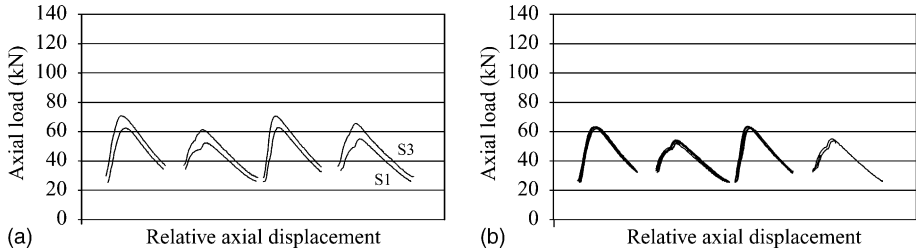

Fig. 12. Secondary folding phase cycle section comparison Configuration A response—S1 and S3 specimens: (a) S1-7 and S3-18 specimens and (b) S1 specimens.

Table 3
Crush characteristics—secondary folding phase, alloy composition and microstructure study—S1-7 and S3-18 specimens

		Cycle no.	Load (kN)					P_{m1} / P_{m2} (kN)	Cycle δ_1, δ_2 (cm)	EA_1 / EA_2 (kN cm)
			P_{s-1}	P_{s-2} / P_{s-6}	P_{s-3} / P_{s-7}	P_{s-4} / P_{s-8}	P_{s-5} / P_{s-9}			
Progressive axial crush study										
S1-7	Pt. 9	1	24.8	63.2	33.9	52.8	25.4	44.3	4.92	218
		2		62.6	32.6	55.4	25.4	44.1	4.97	219
Alloy composition and microstructure study										
S3-18		1	29.3	71.0	36.5	61.9	28.0	49.8	5.18	258
		2		71.0	35.8	65.8	28.7	50.2	5.17	260
Minimum percent increase of S3 values with respect to S1 values										
			18	12	8	17	10	12	4	18

ε martensite formation to further understand material performance during the axial crush fold formation process for AISI 304 SS.

Finally, for square box components, mathematical models have been generated in past research investigations to relate axial crush characteristics to geometric and material parameters and to predict performance. The resulting equations have been based on modeling the mechanics and kinematics of the folding process. In particular, several equations for the mean crushing strength, P_m, have been developed for a square column assuming homogeneous, isotropic, rigid perfectly plastic material with equivalent time- and temperature-independent behavior in uniaxial tension and compression and no corner geometry effect. For a constant but otherwise arbitrary energy equivalent flow stress, σ_o, such that $\sigma_y \leqslant \sigma_o \leqslant \sigma_u$, where σ_y and σ_u are the true "yield" stress and true ultimate stress, respectively, and $M_o = \sigma_o t^2/4$, the equations are of the form:

$$P_m/M_o = C(b/t)^x \tag{3}$$

Values for the coefficient, C, and exponent, x, have been derived for an ideal thin-walled tube for which folds flatten completely, $C = 38.12$ and $x = 0.33$ (Wierzbicki and Abramowicz, 1983; Abramowicz and Jones, 1984) and with an adjustment for an effective crushing distance, $C = 52.22$ and $x = 0.33$ (Abramowicz and Jones, 1984). Based on an empirically derived equation for structural effectiveness, and setting $\sigma_o = \sigma_u$, $C = 68$ and $x = 0.20$ (Magee and Thornton, 1979). For mild steel and using a power law to approximate the stress–strain relation and assuming 0.3 for the ultimate strain of the material, the energy equivalent flow stress for a progressively collapsing rectangular column has been bounded by $0.9\sigma_u \leqslant \sigma_o \leqslant 0.95\sigma_u$ (Wierzbicki and Abramowicz, 1989).

The results of the second study in the current investigation provide symmetric axial crush mode data for a single configuration response of specimens with different AISI 304 SS material strength levels. Unfortunately, direct input of the data into the different models based on Eq. (3) is not valid because several modeling assumptions are incorrect for the AISI 304 SS axial crush specimens. Microstructure around the cross-section is non-uniform due to the cold-forming operations and the weld seam. Significant stain hardening is characteristic of the material. Because of the occurrence of the martensitic transformation in the corner fold areas, equal material response in tension and compression cannot necessarily be assumed. Furthermore, the fold formation process for the tube specimens deviates from that of a perfect square section because of the rounded corner geometry. However, it is interesting to note that for all three equations, when the experimental mean crushing loads for the S1-7 and the S3-18 specimens were used to back-calculate flow stress, the calculated values were between the corresponding true uniaxial tension "yield" and ultimate stresses for both materials. Additionally, for the two models with $C \geqslant 50$, the predicted flow stresses were closer to the true yield stress and corresponded to engineering strains less than 0.2. In the future, detailed studies of the response of AISI 304 SS with respect to the critical stress/strain states involved in the fold formation process are required. In addition, axial crush experiments on components for which the model assumptions are valid are necessary to evaluate the mathematical model predictions for Configuration A response and other configuration responses of the symmetric axial crush mode of the square box component.

4. Conclusions and future research

An experimental investigation of the axial crush response of thin-walled, ductile metallic alloy, square box components was performed. Test specimens were taken from two lengths, designated S1 and S3, of welded, AISI 304 stainless steel tubing with constant geometry. All testing was quasi-static and performed at room temperature. The investigation consisted of two parts: a progressive axial crush study, and an alloy composition and microstructure study.

In the progressive axial crush study, test specimens were cut from the S1 tube length. Removable grooved end caps provided consistent tube specimen end support conditions. Collapse initiators consisted of a double set of transverse, full sidewall width, machined grooves in opposite sidewalls with a vertical offset for groove pairs in adjacent sidewalls. The initiators were used to produce consistent collapse initiation location and initial fold formation, and to promote the specific axial crush configuration response in the secondary folding phase. Using the results from a prototype S1 test specimen that had undergone the specific configuration response, nine deformation points in second cycle of the secondary folding phase were chosen from the specimen's load–displacement curve. Ten S1 test specimens were selected and each specimen was axially compressed to a pre-selected deformation point.

All specimens underwent symmetric axial crush mode response. Consistent fold appearance and load–displacement curve shape matches indicated that nine of the ten specimens had undergone the specific axial crush configuration response of the prototype specimen and the set of specimens represented the permanent deformations of the fold formation process for the second cycle of the configuration's secondary folding phase. For the configuration response specimens, good agreement was obtained for crush characteristic values in the initial phase. Using an average value basis, the maximum percent difference was less than or equal to 10% for the peak load, 7% for load magnitudes and 3% for mean load, displacement, and energy absorption. Very good agreement was obtained for crush characteristic values in the first cycle of the secondary folding phase. Using an average value basis, the percent difference was less than or equal to 3% for maximum load magnitudes, 6% for minimum load magnitudes and 3% for mean load, displacement, and energy absorption.

For the alloy composition and microstructure study, the same experimental methodology as in the first study was used to obtain the specific axial crush configuration response in a tube specimen from tube length S3, and therefore to isolate the effect of material parameters on axial crush performance. The axial crush response for the S3 specimen was compared to an S1 specimen that had been crushed through the second cycle of the secondary folding phase. Both fold appearance and general load–displacement curve shapes were similar for the two specimens and indicated that both specimens had undergone the same configuration response. However, the higher concentration of carbon and smaller grain size in the S3 material resulted in an overall vertical upward shift of the cycle section curves and minimum increases of 8% for load magnitudes, 12% for mean load and 18% for energy absorption for the secondary fold formation phase of the configuration response.

Results of the investigation demonstrate the ability to restrict symmetric axial crush mode response to a specific configuration consisting of a fold formation process and the corresponding load–displacement curve. Therefore, for the box component tube specimens with constant geometry and material, repeatable load magnitudes and energy absorption process can be ensured. Moreover, uniformity was achieved from specimen to specimen of a commercially-produced product and therefore, it was possible to isolate and examine the effect of material parameters on the axial crush configuration response.

For future research efforts, if end constraints and collapse initiators are used to restrict response of box component specimens to a specific configuration, studies can focus on material performance aspects of axial crush response. For instance, the progressive axial crush study specimen set is being used to study plastic deformation in critical sections during the secondary phase fold formation process of the Configuration A response for the AISI 304 SS material. Similar studies using the Configuration A response are planned for box components of other ductile metallic alloy materials.

In addition, research on the secondary folding phase crush characteristic differences for various configuration responses of a specific component could be performed using modifications to the collapse initiator design. In general, research investigations are also needed to develop methods to control the entire axial crush configuration response, modify foldline paths, and optimize the energy absorption process for an axial crush component. These methods could then be used as a basis to develop the more complex methods required to control the energy absorption paths in general three dimensional structures for

applications such as crashworthiness capability, independent of angle of collision, and blast resistance of structures for increased threat levels.

Acknowledgements

The authors gratefully acknowledge the generous support and encouragement of the research work by the Department of Civil and Environmental Engineering at the University of California at Berkeley. In particular, we wish to extend our appreciation to Dr. Lev Stepanov for his contributions to the experimental testing effort. Finally, we thank the Chief of Engineers for permission to publish this paper.

References

Abah, L., Limam, A., Dejeammes, M., 1998. Effects of cutouts on static and dynamic behaviour of square aluminium extrusions. In: Jones, N., Talaslidis, D.G., Brebbia, C.A., Manolis, G.D. (Eds.), Structures Under Shock and Impact V—SUSI 98. Computational Mechanics Publications, Southampton, UK, pp. 133–142.

Abramowicz, W., Jones, N., 1984. Dynamic axial crushing of square tubes. International Journal of Impact Engineering 2 (2), 179–208.

Abramowicz, W., Jones, N., 1986. Dynamic progressive buckling of circular and square tubes. International Journal of Impact Engineering 4 (4), 243–270.

Abramowicz, W., Jones, N., 1997. Transition from initial global bending to progressive buckling of tubes loaded statically and dynamically. International Journal of Impact Engineering 19 (5–6), 415–437.

Abramowicz, W., Wierzbicki, T., 1979. A kinematic approach to crushing of shell structures. In: Record of Conference Papers—Annual Petroleum and Chemical Industry Conference—International Conference on Vehicle Structural Mechanics, 3rd, October 10–12, 1979, Troy, MI, P-83 (790992). Society of Automotive Engineers, Warrendale, PA, pp. 211–223.

Andrews, K.R.F., England, G.L., Ghani, E., 1983. Classification of the axial collapse of cylindrical tubes under quasi-static loading. International Journal of Mechanical Sciences 25 (9–10), 687–696.

Angel, T., 1954. Formation of martensite in austenitic stainless steels—effects of deformation, temperature, and composition. Journal of the Iron and Steel Institute (May), 402–412.

ASTM Designation: A 666-99, 2000. Standard specification for annealed or cold-worked austenitic stainless steel sheet, strip, plate, and flat bar. Annual Book of ASTM Standards 2000, Section 1, Iron and Steel Products, Volume 01.03, Steel—Plate, Sheet, Strip, Wire; Stainless Steel Bar. ASTM, West Conshohocken, PA, 360–366.

ASTM Designation: E8-96 a, 1997. Standard Test Methods for Tension Testing of Metallic Materials, Annual Book of ASTM Standards 1997, Section 3, Metals, Test Methods and Analytical Procedures, Volume 03.01, Metals—Mechanical Testing; Elevated and Low Temperature Tests; Metallography. ASTM, West Conshohocken, PA, 56–76.

Bleich, F., 1952. Buckling Strength of Metal Structures. McGraw-Hill Book Company, Inc., New York, NY.

Buehler Consumables Buyer's Guide, 1999. Buehler Ltd., Lake Bluff, IL, USA.

Chou, C.C., 1983. The measurement of impact forces under dynamic crush using a drop tower test facility. In: International Congress and Exposition, February 28–March 4, 1983, Detroit, MI (830467). Society of Automotive Engineers, Warrendale, PA, pp. 1–16.

Coppa, A.P., 1968. New ways to soften shock. Machine Design (March 28), 130–140.

DiPaolo, B.P., 1992. An experimental and analytical investigation of the axial crush of an aluminum box section. Unpublished M.S. Thesis, Department of Civil Engineering, School of Engineering, University of Pittsburgh, Pittsburgh, PA.

DiPaolo, B.P., 2000. An experimental investigation on the axial crush of a thin-walled, stainless steel box component. Ph.D. Dissertation, Department of Civil and Environmental Engineering, College of Engineering, University of California, Berkeley, CA.

Ezra, A.A., Fay, R.J., 1972. An assessment of energy absorbing devices for prospective use in aircraft impact situations. In: Herrmann, G., Perrone, N. (Eds.), Dynamic Response of Structures—Proceedings of a Symposium, June 28 and 29, 1971, Stanford, CA. Pergamon Press, New York, pp. 225–246.

Foreman, E.A., 1999. (November 19). Laboratory certificate number 5003.1578. FTI Anamet, Hayward, CA, USA.

Gray, R.J., Holbert, R.K., Thrasher, T.H., 1985. Microstructural analysis for series 300 stainless steel sheet welds and tensile samples. In: Northwood, D.O., White, W.E., Vander Voort, G.F. (Eds.), Proceedings of the Sixteenth Annual Technical Meeting of the International Metallographic Society—Corrosion, Microstructure and Metallography. In: Microstructural Science, vol. 12. ASM International, Materials Park, OH, pp. 345–370.

Griffiths, A.J., Wright, J.C., 1969. Mechanical properties of austenitic and metastable stainless steel sheet and their relationships with pressforming behaviour. In: Stainless Steels—Proceedings of the Conference on Stainless Steels for the Fabricator and User, September 10–12, 1968, Birmingham, UK, 117. Staples Printers Limited for The Iron and Steel Institute, London, pp. 51–65.

Grimm, T.R., Johnson, D.M., Kajander, J.E., Viegelahn, G.L., 1988. An Investigation of the Crush Characteristics of Flanged Sheet Metal Columns (880904). Society of Automotive Engineers, Warrendale, PA. pp. 171–177.

Gupta, N.K., Gupta, S.K., 1993. Effect of annealing, size and cut-outs on axial collapse behaviour of circular tubes. International Journal of Mechanical Sciences 35 (7), 597–613.

Hecker, S.S., Stout, M.G., Staudhammer, K.P., Smith, J.L., 1982. Effects of strain state and strain rate on deformation-induced transformation in 304 stainless steel: Part I. Magnetic measurements and mechanical behavior. Metallurgical Transactions A 13 (April), 619–626.

Hordijk, W., 2003. Written Communication. Phoenix Tube Co., Inc., Bethlehem, PA, USA.

Horton, W.H., Bailey, S.C., Edwards, A.M., 1966. Nonsymmetric buckle patterns in progressive plastic buckling. Experimental Mechanics (September), 433–444.

Johnson, W., Reid, S.R., 1978. Metallic Energy Dissipating Systems. Applied Mechanics Reviews 31 (3), 277–288.

Johnson, W., Soden, P.D., Al-Hassani, S.T.S., 1977. Inextensional collapse of thin-walled tubes under axial compression. Journal of Strain Analysis 12 (4), 317–330.

Jones, N., 1997. Structural Impact. Cambridge University Press, Cambridge, UK.

Kindervater, C., 1981. Quasi-static and dynamic crushing of energy absorbing materials and structural components with the aim of improving helicopter crashworthiness. In: Seventh European Rotorcraft and Powered Lift Aircraft Forum (66), September 8–11, 1981, Stuttgart, Germany, pp. 1–26.

Lampinen, B.E., Jeryan, R.A., 1983. Effectiveness of Polyurethane Foam in Energy Absorbing Structures (820494). Society of Automotive Engineers, Warrendale, PA. pp. 2059–2076.

Langseth, M., Berstad, T., Hopperstad, O.S., Clausen, A.H., 1994. Energy absorption in axially loaded square thin-walled aluminium extrusions. In: Bulson, P.S. (Ed.), Structures Under Shock and Impact III—Proceedings of the Third International Conference, SUSI/94, 1st–3rd June, 1994, Madrid, Spain. Computational Mechanics Publications, Southampton, UK, pp. 401–410.

Logan, R.W., Burger, M.J., McMichael, L.D., Parkinson, R.D., 1993. Crashworthiness analysis using advanced material models in Dyna3D. In: Crashworthiness and Occupant Protection in Transportation Systems 1993—The 1993 ASME Winter Annual Meeting, November 28–December 3, 1993, New Orleans, LA, AMD169/BED 25. The American Society of Mechanical Engineers, New York, pp. 127–136.

Macaulay, M.A., Redwood, R.G., 1964. Small scale model railway coaches under impact. Engineer 218, 1041–1046.

Magee, C.L., Thornton, P.H., 1979. Design Considerations in Energy Absorption by Structural Collapse (780434). Society of Automotive Engineers, Warrendale, PA. pp. 2041–2055.

Mahmood, H.F., Paluszny, A., 1981. Design of thin walled columns for crash energy management—their strength and mode of collapse. In: Proceedings of Fourth International Conference on Vehicle Structural Mechanics (811302). Society of Automotive Engineers, Warrendale, PA, pp. 7–18.

Mahmood, H.F., Paluszny, A., 1982. Stability of plate-type box columns under crush loading. In: Kamal, M.M., Wolf, J.A. (Eds.), Computational Methods in Ground Transportation Vehicles—The Winter Annual Meeting of the American Society of Mechanical Engineers, November 14–19, 1982, Phoenix, AZ. American Society of Mechanical Engineers, New York, pp. 17–33.

Mallock, A., 1908. Note on the instability of tubes subjected to end pressure, and on the folds in a flexible material. Proceedings of the Royal Society A 81 (December), 388–393.

Mamalis, A.G., Johnson, W., 1983. The quasi-static crumpling of thin-walled circular cylinders and frusta under axial compression. International Journal of Mechanical Sciences 25 (9–10), 713–732.

Mamalis, A.G., Johnson, W., Viegelahn, G.L., 1984. The crumpling of steel thin-walled tubes and frusta under axial compression at elevated strain-rates: some experimental results. International Journal of Mechanical Sciences 26 (11/12), 537–547.

Mamalis, A.G., Viegelahn, G.L., Manolakos, D.E., Johnson, W., 1986. Experimental investigation into the axial plastic collapse of steel thin-walled grooved tubes. International Journal of Impact Engineering 4 (2), 117–126.

Mamalis, A.G., Manolakos, D.E., Viegelahn, G.L., 1989. The axial crushing of thin PVC tubes and frusta of square cross-section. International Journal of Impact Engineering 8 (3), 241–264.

Marshall, N.S., Nurick, G.N., 1998. The effect of induced imperfections on the formation of the first lobe of symmetric progressive buckling of thin-walled square tubes. In: Jones, N., Talaslidis, D.G., Brebbia, C.A., Manolis, G.D. (Eds.), Structures Under Shock and Impact V—SUSI 98. Computational Mechanics Publications, Southampton UK, pp. 155–168.

McGregor, I.J., Meadows, D.J., Scott, C.E., Seeds, A.D., 1993. Impact performance of aluminium structures. In: Jones, N., Wierzbicki, T. (Eds.), Structural Crashworthiness and Failure, vol. 10. Elsevier Applied Science, London, pp. 385–421.

Meng, Q., Al-Hassani, S.T.S., Soden, P.D., 1983. Axial crushing of square tubes. International Journal of Mechanical Sciences 25 (9–10), 747–773.

Ohkubo, Y., Akamatsu, T., Shirasawa, K., 1974. Mean Crushing Strength of Closed-Hat Section Members (740040). Society of Automotive Engineers, Warrendale, PA. pp. 223–232.

Powell, G.W., Marshall, E.R., Backofen, W.A., 1958. Strain hardening of austenitic stainless steel. Transactions of the ASM 50, 478–497.

Pugsley, A., 1960. The crumpling of tubular structures under impact conditions. In: Symposium on the Use of Aluminium in Railway Rolling Stock. The Institution of Locomotive Engineers and the Aluminium Development Association, London. pp. 33–41.

Pugsley, A., Macaulay, M., 1960. The large-scale crumpling of thin cylindrical columns. The Quarterly Journal of Mechanics and Applied Mathematics 13 (Pt. 1), 1–9.

Redwood, R.G., 1964. On the buckling of thin walled tubes under axial impact. Journal of the Royal Aeronautical Society 68 (7), 418–419.

Reid, S.R., Reddy, T.Y., 1986a. Axially loaded metal tubes as impact energy absorbers. In: Bevilacqua, L., Feijoo, R., Valid, R. (Eds.), Inelastic Behaviour of Plates and Shells—International Union of Theoretical and Applied Mechanics (IUTAM) Symposium, August 5–9, 1985, Rio de Janeiro, Brazil. Springer-Verlag, Berlin, pp. 569–595.

Reid, S.R., Reddy, T.Y., 1986b. Static and dynamic crushing of tapered sheet metal tubes of rectangular cross-section. International Journal of Mechanical Sciences 28 (9), 623–637.

Reid, S.R., Reddy, T.Y., Gray, M.D., 1986. Static and dynamic axial crushing of foam-filled sheet metal tubes. International Journal of Mechanical Sciences 28 (5), 295–322.

Ren, W., Mingbao, H., Zhuping, H., Qingchun, Y., 1983. An experimental study on the dynamic axial plastic buckling of cylindrical shells. International Journal of Impact Engineering 1 (3), 249–256.

Ryerson Stock List—Steel, Aluminum, Nickel, Plastics, Copper, Brass—Processing and Fabricating, 1991. Joseph T. Ryerson & Son, Inc., Chicago, USA.

Singace, A.A., 1999. Axial crushing analysis of tubes deforming in the multi-lobe mode. International Journal of Mechanical Sciences 41, 865–890.

Soden, P.D., Al-Hassani, S.T.S., Johnson, W., 1974. The Crumpling of Polyvinylchloride Tubes Under Static and Dynamic Axial Loads. Institute of Physics Conference Series No. 21, Oxford, 327–338.

Tani, M., Funahashi, A., 1978. Energy absorption by the plastic deformation of body structural members. In: SAE Congress and Exposition, Cobo Hall, February 27–March 3, 1978, Detroit, MI (780368). Society of Automotive Engineers, Warrendale, PA, pp. 1–12.

Thornton, P.H., 1975. Static and dynamic collapse characteristics of scale model corrugated tubular sections. Transactions of the ASME—Journal of Engineering Materials and Technology 75 (October), 357–362.

Thornton, P.H., 1979. Energy absorption by structural collapse in dual phase steel tubes. Metallurgical Transactions A 10 (August), 1199–1201.

Thornton, P.H., Magee, C.L., 1977. The interplay of geometric and materials variables in energy absorption. Transactions of the ASME—Journal of Engineering Materials and Technology 99 (2), 114–120.

Toda, K., Gondoh, H., Takechi, H., Usuda, M., 1976. Absorbed energy during compression and crushing of high strength steel sheets. Metallurgical Transactions A 7 (November), 1637–1642.

VanKuren, R.C., Scott, J.E., 1978. Energy Absorption of High-Strength Steel Tubes Under Impact Crush Conditions (770213). Society of Automotive Engineers, Warrendale, PA. pp. 947–954.

Wierzbicki, T., Abramowicz, W., 1983. On the crushing mechanics of thin-walled structures. Transactions of the ASME—Journal of Applied Mechanics 50 (4a), 727–734.

Wierzbicki, T., Abramowicz, W., 1989. The mechanics of deep plastic collapse of thin-walled structures. In: Wierzbicki, T., Jones, N. (Eds.), Structural Failure, vol. 9. John Wiley, New York, pp. 281–329.

Wierzbicki, T., Molnar, C., Matolcsy, M., 1978. Experimental–theoretical correlation of dynamically crushed components of bus frame structure. In: 17th FISITA Congress (785124). Society of Automotive Engineers, Warrendale, PA, pp. 1673–1685.

Wong, H.F., Rhodes, J., Zaras, J., Ujihashi, S., 1997. Experimental investigation of static progressive crushing of closed-hat section members. In: Gupta, N.K. (Ed.), Plasticity and Impact Mechanics. New Age International Ltd., New Delhi, pp. 250–272.

Yamaguchi, S., Kato, H., Okazaki, T., 1985. Efficient energy absorption of automobile side rails. In: Tenth International Technical Conference on Experimental Safety Vehicles, July 1–4, 1985, Oxford, England. US Department of Transportation, National Highway Traffic Safety Administration, pp. 321–326.

Yamaya, M., Tani, M., 1971 (June). Energy absorption by the plastic deformation of sheet metal columns with box-shaped cross section. Technical Review. Mitsubishi Heavy Industries, Ltd., pp. 59–66.